Inorganic Chemistry Article

Inorg. Chem. 2011, 50, 1879–1888 1879
DOI: 10.1021/ic102273n

Activation of Carbon Dioxide by Divalent Tin Alkoxides Complexes

Lorenzo Ferro, Peter B. Hitchcock, Martyn P. Coles, Hazel Cox, and J. Robin Fulton*

Department of Chemistry, University of Sussex, Falmer, Brighton BN1 9QJ, U.K.

Received November 12, 2010

A series of terminal tin(II) alkoxides have been synthesized utilizing the bulky β-diketiminate ligand [{N(2,6-$_i$Pr$_2$C$_6$H$_3$)-C(Me)}$_2$CH] (BDI). The nucleophilicities of these alkoxides have been examined, and unexpected trends were observed. For instance, (BDI)SnOR only reacts with highly activated aliphatic electrophiles such as methyl triflate, but reacts reversibly with carbon dioxide. Both the rate of reaction and the degree of reversibility is dependent upon minor changes in the alkoxide ligand, with the bulkier *tert*-butoxide ligand displaying slower reactivity than the corresponding isopropyl ligand, although the latter system is a more exergonic reaction. Density Function Theory (DFT) calculations show that the differences in the reversibility of carbon dioxide insertion can be attributed to the ground-state energy differences of tin alkoxides while the rate of reaction is attributed to relative bond strengths of the Sn—O bonds. The mechanism of carbon dioxide insertion is discussed.

Introduction

The activation of carbon dioxide by metal complexes has recently received fresh attention because of the obvious implication for carbon dioxide sequestering or converting carbon dioxide into a useful carbon feedstock. Metal complexes used in carbon dioxide activation generally possess nucleophilic ligands such as alkoxides and amides; in these systems, carbon dioxide is inserted into the M—O or M—N bond to form a metallo-alkylcarbonate (or -alkylcarbamate) complex.[1−11] In general, most metal alkoxide complexes react reversibly with carbon dioxide,[1,3−9] presumably because of similar M—O bond strengths of the metal alkoxide and metallo-alkylcarbonate. Metal amide complexes exhibit both reversible[12] and irreversible reactivity with carbon dioxide.[1,10] The mechanism for carbon dioxide insertion into M—O or M—N bonds has been postulated to occur via a four-membered transition state in which the alkoxide or amide ligand acts as a nucleophile onto the electrophilic carbon atom concurrent with coordination of one of the carbon dioxide oxygen atoms to the metal center and a weakening of the M—O and the C=O bonds (Scheme 1). An open coordination site is unnecessary for this nucleophilic insertion reaction[13] and the driving force for this reaction is generally thought to be the strong nucleophilicity of the alkoxide or amide ligand.[1,9,11]

Although tin(IV) alkoxides complexes are known to react with carbon dioxide,[7,14] the reactivity of the less Lewis acidic tin(II) alkoxides has not been explored outside of lactide polymerization studies.[15,16] Divalent tin has one of the lowest aqueous acidities of any metal species (pK_a = 2),[17,18] significantly lower than what is predicted based upon electrostatic parameters. As such, the resultant tin hydroxide species is very weakly basic and should not exhibit nucleophilic behavior. As the reactivity of alkoxides is similar to that of hydroxides, divalent tin alkoxides should also be very weakly basic and non-nucleophilic.

We have recently synthesized a series of monomeric divalent lead alkoxides complexes utilizing the bulky β-diketiminate monoanionic ligand [{N(2,6-^{i}Pr$_2$C$_6$H$_3$)C(Me)}$_2$CH]$^-$ (BDI) to stabilize the low-coordinate complexes.[4,19] As with divalent

*To whom correspondence should be addressed. E-mail: j.r.fulton@sussex.ac.uk.

(1) Simpson, R. D.; Bergman, R. G. *Organometallics* **1992**, *11*, 4306.
(2) Darensbourg, D. J.; Sanchez, K. M.; Rheingold, A. L. *J. Am. Chem. Soc*. **1987**, *109*, 290.
(3) Darensbourg, D. J.; Sanchez, K. M.; Reibenspies, J. H.; Rheingold, A. L. *J. Am. Chem. Soc*. **1989**, *111*, 7094.
(4) Tam, E. C. Y.; Johnstone, N. C.; Ferro, L.; Hitchcock, P. B.; Fulton, J. R. *Inorg. Chem*. **2009**, *48*, 8971.
(5) Tsuda, T.; Saegusa, T. *Inorg. Chem*. **1972**, *11*, 2561.
(6) Chisholm, M. H.; Cotton, F. A.; Extine, M. W.; Reichert, W. W. *J. Am. Chem. Soc*. **1978**, *100*, 1727.
(7) Choi, J.-C.; Sakakura, T.; Sako, T. *J. Am. Chem. Soc*. **1999**, *121*, 3793.
(8) Mandal, S. K.; Ho, D. M.; Orchin, M. *Organometallics* **1993**, *12*, 1714.
(9) Darensbourg, D. J.; Lee, W. Z.; Phelps, A. L.; Guidry, E. *Organometallics* **2003**, *22*, 5585.
(10) Boyd, C. L.; Clot, E.; Guiducci, A. E.; Mountford, P. *Organometallics* **2005**, *24*, 2347.
(11) Brombacher, H.; Vahrenkamp, H. *Inorg. Chem*. **2004**, *43*, 6042.
(12) McCowan, C. S.; Groy, T. L.; Caudle, M. T. *Inorg. Chem*. **2002**, *41*, 1120.
(13) Darensbourg, D. J.; Mueller, B. L.; Bischoff, C. J.; Chojnacki, S. S.; Reibenspies, J. H. *Inorg. Chem*. **1991**, *30*, 2418.
(14) Kizlink, J. *Collect. Czech. Chem. Commun*. **1993**, *58*, 1399.
(15) Dove, A. P.; Gibson, V. C.; Marshall, E. L.; White, A. J. P.; Williams, D. J. *Chem. Commun*. **2001**, 283.
(16) Dove, A. P.; Gibson, V. C.; Marshall, E. L.; Rzepa, H. S.; White, A. J. P.; Williams, D. J. *J. Am. Chem. Soc*. **2006**, *128*, 9834.
(17) Burgess, J. *Metal Ions in Solution*; Ellis Horwood Ltd: Chichester, U.K., 1978.
(18) Cox, H.; Stace, A. J. *J. Am. Chem. Soc*. **2004**, *126*, 3939.
(19) Fulton, J. R.; Hitchcock, P. B.; Johnstone, N. C.; Tam, E. C. Y. *Dalton Trans*. **2007**, 3360.

Scheme 1. Insertion of Carbon Dioxide into a M–O Bond via a Four-Membered Transition State. R is Either an Aliphatic or Aromatic Group

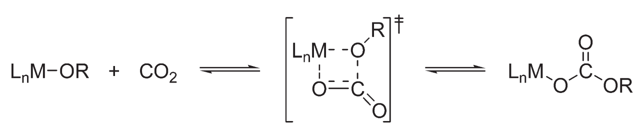

tin, divalent lead has a low aqueous acidity of 7.2.[17] As such, lead hydroxides, and by analogy, lead alkoxides, should only be weakly nucleophilic. Our (BDI)PbOR (R = *i*Pr, *s*Bu, and *t*Bu) complexes displayed only sluggish reactivity with methyl iodide, suggesting that the lead alkoxides are non-nucleophilic. However, these lead alkoxide complexes do react readily and reversibly with carbon dioxide to form lead-alkylcarbonate complexes. Both the rate of reaction as well as the degree of reversibility was found to be dependent upon the alkoxide substituent. For instance, when (BDI)PbO^{i}Pr was treated with carbon dioxide, quantitative formation of the corresponding carbonate was observed. In contrast, when the alkoxide substituent was *tert*-butoxide, (BDI)PbO^{t}Bu, the carbonate was only observed in solution and application of reduced pressure resulted in the reformation of the alkoxide. Although our investigations of the lead system allowed for a qualitative study on these observations, a more quantitative examination was thwarted by decomposition of the *tert*-butyl carbonate, preventing accurate equilibrium measurements. Fortunately, the isostructural tin system has similar, but slower, reactivity patterns to that of the lead alkoxides; as such, we report the results of the thermodynamic and computational studies for the insertion of carbon dioxide into a Sn(II)–O bond, as well as factors behind the apparent non-nucleophilicity of these group 14 alkoxide complexes.

Results

Synthesis and Reactivity. The synthesis of tin isopropoxide (BDI)SnO^{i}Pr (**2a**) has been reported elsewhere.[15] Treatment of a THF solution of (BDI)SnCl(**1**) with KO^{s}Bu and KO^{t}Bu affords tin alkoxides (BDI)SnO^{s}Bu (**2b**) and (BDI)SnO^{t}Bu (**2c**), respectively, after three days at room temperature (eq 1). The X-ray crystal structures were determined for **2b** and **2c**; Figure 1 shows the ORTEP diagrams of *sec*-butoxide **2b** and *tert*-butoxide **2c**. Selected bond lengths and angles for **2a**, **2b**, and **2c** are reported in Table 1 and data collection parameters for **2b** and **2c** are given in Table 2. Analogous to the solid-state structures reported for **2a**, as well as the isostructural lead compounds, a pyramidal ligand arrangement is observed around the tin metal center. This geometry is presumably a result of the relativistic contraction of the 5*s* tin orbital, resulting in minimal hybridization of the *s* and *p* orbitals, thus producing a stereochemically active lone pair.[20,21] The alkoxy group in the solid state structure of **2a**, **2b**, and **2c** points away from the BDI-Sn core and, in contrast to the (BDI)SnCl precursor, the Sn and alkoxide ligand lie on opposite sides of the BDI backbone N_2C_3 plane. Only minor variations are observed between the tin alkoxide complexes, such as an increase in the Sn–O bond length with the increasing bulk of the alkoxy ligand, and a very slight increase of pyramidalization around the tin metal center with increasing bulk of the alkoxy ligand.

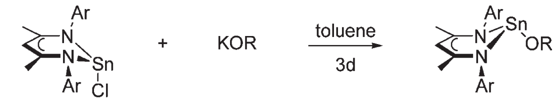

(1)

Ar = 2,6-*i*Pr$_2$-C$_6$H$_3$

1

2a, R = *i*Pr
2b, R = *s*Bu
2c, R = *t*Bu

The reactivity of tin alkoxides **2a**, **2b**, and **2c** with aliphatic electrophiles was examined. No reactivity was observed between the tin alkoxides and methyl iodide, even at elevated temperatures. This is in contrast to the apparent nucleophilic reactivity observed with the isostructural lead alkoxides complexes; formation of (BDI)PbI and the corresponding methyl ether was observed upon heating a solution of (BDI)PbOR with methyl iodide.[4] In addition, this lack of reactivity is also in contrast to transition metal alkoxide complexes in which facile reactivity with aliphatic electrophiles is observed.[11,22] Addition of a more reactive electrophile, methyl triflate, to **2a**, **2b**, and **2c** does result in apparent nucleophilic behavior of the alkoxides as the known (BDI)SnOTf complex (**3**) is formed along with the corresponding methyl ether (eq 2).[23] Interestingly, the half-life for this reaction is dependent upon the alkoxide group, with the tin isopropoxide **2a** proving to be the most reactive ($t_{1/2}$ = 8 min), tin *sec*-butoxide **2b** to be slightly slower ($t_{1/2}$ = 15 min) and the tin *tert*-butoxide **2c** to be the most sluggish ($t_{1/2}$ = 150 min).

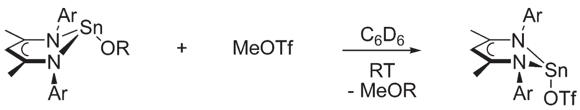

(2)

2a - 2c **3**

In contrast to aliphatic electrophiles, compounds **2a**, **2b**, and **2c** readily react with unsaturated electrophiles. Although addition of CS_2 and phenylisocyanate to the tin alkoxide complexes gave intractable product mixtures, treatment of isopropoxide **2a** with maleic anhydride results in ring opened product (BDI)SnO$_2$CCHCHCO$_2$^{i}Pr **4** in 87% yield (eq 3). The X-ray crystal structure was determined (Figure 2); the bond lengths and bond angles are listed in Table 3 and data collection parameters are listed in Table 2. Although this reactivity is known for transition metal alkoxides this is a rare example a structurally characterized terminal metal maleate complex.[24,25] The unit cell consists of two independent molecules that differ in the conformation of the maleate ligand. In both molecules, the metal center and the maleate ligand lie on the same side of the N_2C_3 backbone plane and the ligand bond angles around the metal center are more acute than in the alkoxide examples. The Sn–O bond length is longer than the alkoxide analogues, potentially due to a stabilizing Sn···O2 interaction

(20) Chen, M.; Fulton, J. R.; Hitchcock, P. B.; Johnstone, N. C.; Lappert, M. F.; Protchenko, A. V. *Dalton Trans.* **2007**, 2770.
(21) For a good description of this hybridization, see reference 16.
(22) Fulton, J. R.; Holland, A. W.; Fox, D. J.; Bergman, R. G. *Acc. Chem. Res.* **2002**, *35*, 44.
(23) Ding, Y.; Roesky, H. W.; Noltemeyer, M.; Schmidt, H.-G.; Power, P. P. *Organometallics* **2001**, *20*, 1190.
(24) Cuesta, L.; Hevia, E.; Morales, D.; Perez, J.; Riera, L.; Miguel, D. *Organometallics* **2006**, *25*, 1717.
(25) Fulton, J. R.; Sklenak, S.; Bouwkamp, M. W.; Bergman, R. G. *J. Am. Chem. Soc.* **2002**, *124*, 4722.

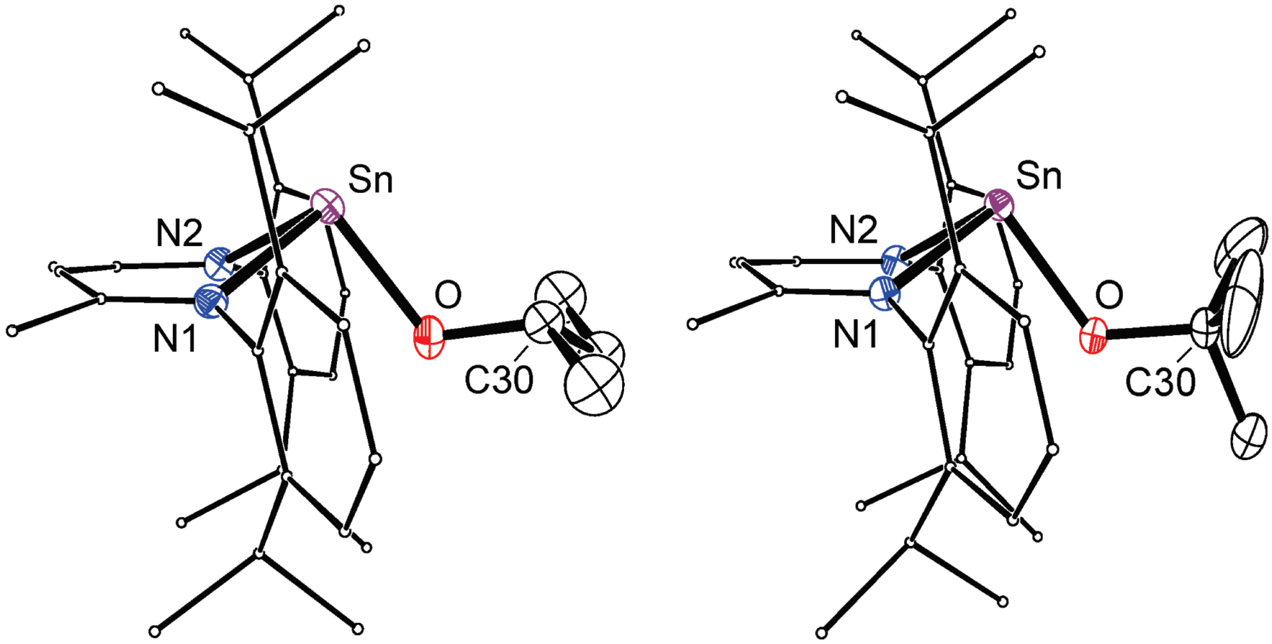

Figure 1. ORTEP diagrams of (BDI)SnO^{t}Bu **2b** (left) and (BDI)SnO^{t}Bu **2c** (right) with H atoms omitted and BDI aryl groups C atoms minimized for clarity; ellipsoid probability shown at 30%.

Table 1. Selected Bond Lengths (Å) and Angles (deg) for Compounds **2a**, **2b**, **2c**, and **2d**

	(BDI)SnO^{i}Pr (**2a**)^a	(BDI)SnO^{s}Bu (**2b**)	(BDI)SnO^{t}Bu (**2c**)	(BDI)SnO^{t}Bu^F (**2d**)
Sn−O	2.000(5)	2.013(3)	2.0179(16)	2.110(2)
Sn−N(1)	2.206(4)	2.202(3)	2.2015(19)	2.1837(16)
Sn−N(2)	2.208(4)	2.202(3)	2.2100(19)	2.1837(16)
O−C(30)	1.418	1.442(7)	1.419(3)	1.360(3)
N(1)−Sn−N(2)	83.6(2)	82.79(11)	83.02(7)	83.53(8)
N(1)−Sn−O(1)	94.1(2)	94.08(12)	92.66(7)	93.65(6)
N(2)−Sn−O(1)	95.2(2)	94.29(12)	93.89(7)	93.65(6)
Sn−O−C(30)^c	118.58	118.1(3)	122.40(16)	128.97(18)
Sn−NCCCN plane	0.938	0.974	0.990	1.056
sum of angles around Sn	272.9	271.16	269.57	270.83
DP (%)^b	97	99	100	99

^{a} See ref 14. ^{b} Degree of pyramidalization, DP (%) = (360 − [sum of angles])/0.9. ^{c} C(16) for **2d**

of 2.954 Å (molecule A) and 2.898 Å (molecule B), which are inside the combined Sn−O van der Waals radii of 3.69 Å.

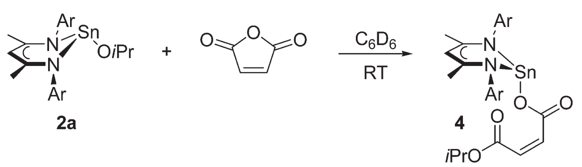

(3)

All three tin alkoxides react with carbon dioxide to give the carbonate insertion product (BDI)SnOCO$_2$R (**5a**−**5c**) (Scheme 2). Although the facile reversibility of this reaction has prevented any solid-state characterization of the tin alkylcarbonates **5**, IR spectroscopy (CCl$_4$) showed the characteristic solution phase carbonyl stretching frequencies at 1621 cm^{-1}. In addition, the ^{13}C NMR spectrum of all three products reveals a resonance at δ 158.7 (**5a**), 158.8 (**5b**), and 158.9 (**5c**) ppm, indicative of a carbonate carbon.[4,8,26] Addition of $^{13}CO_2$ to all of the alkyl carbonates results in an increase of the ^{13}C NMR carbonate resonance. Further conformation of the nature of the product was given by treatment of tin chloride **1** with the potassium salt of monoalkyl carbonate (KO$_2$COR, R = ^{s}Bu, ^{t}Bu), which produced a mixture of tin alkoxide **2** and tin carbonate **5**. Although KO$_2$COR does revert to KOR and CO$_2$, this latter reaction only happens at elevated temperatures.

Interestingly, and similar to the lead alkoxide system, the rate of reaction between **2** and CO$_2$, as well as the observed equilibria between alkoxide **2**, CO$_2$ and metallo-alkylcarbonate **5** is dependent upon the nature of the alkyl group on the alkoxide ligand. For instance, the $t_{1/2}$ for the reaction between isopropoxide **2a** or *sec*-butoxide **2b** with 1 atm of CO$_2$ is < 10 min, and complete conversion to the metallo-alkylcarbonates was observed, but the reaction between *tert*-butoxide **2c** with 1 atm of CO$_2$ is significantly slower and only goes to 74% completion after one week at room temperature.

Equilibrium Studies. To further understand the influence of the alkyl group on the reaction, we investigated both the equilibria formed between the reactants (**2** and CO$_2$) and products (**5**), as well as the rate of reaction between the alkoxides and carbon dioxide. These studies

(26) Campora, J.; Matas, I.; Palma, P.; Alvarez, E.; Graiff, C.; Tiripicchio, A. *Organometallics* **2007**, *26*, 3840.

Table 2. Crystallographic Data for Compounds **2b**, **2c**, **2d**, and **4**

	(BDI)SnO^{s}Bu (**2b**)	(BDI)SnO^{t}Bu (**2c**)^a	(BDI)SnO^{t}Bu^F (**2d**)^b	(BDI)Sn(Ma)O^{i}Pr (**4**)^c
chemical formula	$C_{33}H_{50}N_2OSn$	$C_{33}H_{50}N_2OSn$	$C_{33}H_{41}F_9N_2OSn$	$C_{36}H_{50}N_2O_4Sn$
formula weight	609.44	609.44	771.37	693.47
temp (K)	173(2)	173(2)	173(2)	173(2)
wavelength (Å)	0.71073	0.71073	0.71073	0.71073
cryst size (mm^3)	0.4 × 0.3 × 0.3	0.15 × 0.10 × 0.10	0.16 × 0.08 × 0.06	0.23 × 0.20 × 0.10
cryst syst	triclinic	monoclinic	monoclinic	triclinic
space group	$P\bar{1}$ (No.2)	$P2_1/n$ (No. 14)	$P2_1/m$ (No. 11)	$P\bar{1}$ (No.2)
a (Å)	8.7788(2)	13.3880(2)	8.9128(2)	14.7295(3)
b (Å)	9.8810(2)	16.7487(3)	19.8833(5)	16.2188(2)
c (Å)	20.5060(4)	15.2140(2)	10.4482(2)	17.6171(2)
α (deg)	92.884(2)	90	90	110.624(1)
β (deg)	90.071(1)	107.654(1)	113.394(1)	99.628(1)
γ (deg)	113.948(1)	90	90	108.961(1)
V (Å^3)	1623.12(6)	3250.80(9)	1699.96(7)	3531.49(9)
Z	2	4	2	4
p_c (Mg m^{-3})	1.25	1.25	1.51	1.30
abs coeff (mm^{-1})	0.81	0.81	0.83	0.76
θ range for data collection (deg)	3.64−26.06	3.42−26.01	3.74−27.11	3.40−27.10
measured/indep rflns/R(int)	23390/6364/0.043	45959/6387/0.051	27173/3861/0.063	56849/15530/0.058
rflns with $I > 2\sigma$(I)	5816	5479	3446	12240
data/restraints/params	6364/0/331	6387/0/347	3861/0/263	15530/0/779
GOF on F^2	1.110	1.057	1.023	1.011
final R indices [$I > 2\sigma(I)$]	R_1 = 0.045, R_2 = 0.117	R_1 = 0.029, R_2 = 0.067	R_1 = 0.028, R_2 = 00.059	R_1 = 0.033, R_2 = 0.070
R indices (all data)	R_1 = 0.050, R_2 = 0.121	R_1 = 0.037, R_2 = 0.071	R_1 = 0.035, R_2 = 0.062	R_1 = 0.051, R_2 = 0.076
largst diff. peak and hole (e Å^3)	2.63 and −1.13	0.56 and −0.50	0.36 and −0.35	0.44 and −1.10

^{a} The isobutyl group attached to O is disordered over two partially overlapping orientations with the C30 and C31 alternative positions resolved, and was included with isotropic C atoms. ^{b} The molecule lies on a mirror plane with the alkoxide group disordered over two positions. ^{c} There are two independent molecules in the unit cell that differ in the conformation of the maleate ligand.

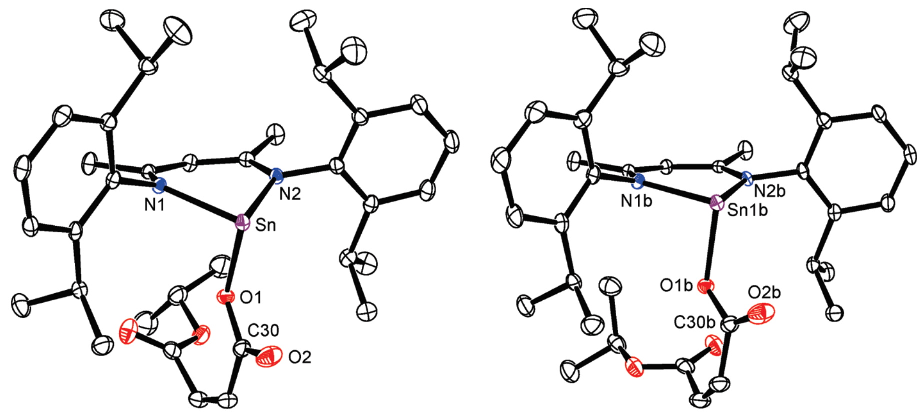

Figure 2. ORTEP diagrams of **4** showing molecule A (left) and molecule B (right) with H atoms omitted for clarity; ellipsoid probability shown at 30%.

Table 3. Selected Bond Lengths and Angles for Compound **4**

molecule A		molecule B	
Sn−O(1)	2.1489(16)	Sn(1b)−O(1b)	2.1534(16)
Sn−N(1)	2.1812(17)	Sn(1b)−N(1b)	2.1866(17)
Sn−N(2)	2.1784(18)	Sn(1b)−N(2b)	2.1851(18)
Sn−O(2)	2.898	Sn(1b)−O(2b)	2.954
N(1)−Sn−N(2)	84.88(7)	N(1b)−Sn(1b)−N(2b)	86.09(7)
O(1)−Sn−N(1)	87.32(7)	O(1b)−Sn(1b)−N(1b)	88.78(6)
O(1)−Sn−N(2)	87.90(7)	O(1b)−Sn(1b)−N(2b)	86.09(7)
sum of angles	260.1	sum of angles	260.96
DP (%)^a	111	DP (%)^a	110

^{a} Degree of pyramidalization, DP (%) = (360 − [sum of angles]/0.9).

are complicated by an additional equilibria between gas phase and solution phase CO_2, which was partially overcome by flooding the reaction with carbon dioxide (1 atm), allowing us to maintain a steady CO_2 concentration and calculate the mole fraction (χ_{CO2}) solubility corrected to a partial pressure of 1.013 bar.[27]

At 298 K and 1 atm of CO_2, the ^{1}H NMR spectrum shows that the tin isopropoxide **2a** is completely converted to the corresponding carbonate **5a**. However, at 313 K, the conversion is only 92%. As such, we used this temperature to perform our comparative equilibrium measurements. Table 4 shows the ratio of **2** and **5** at 313 K, and the calculated K_{eq} and $\Delta G°$ for each system. Although the apparent equilibrium favors the reactants at elevated temperatures, we are unfortunately limited as to a "usable" temperature range due to lack of carbon dioxide solubility data outside of the 283 − 313 K temperature range at barometric pressures.[27] The equilibria between *tert*-butoxide **2c** and metallo-alkylcarbonate **5c** was measured at four different temperatures and the $\Delta H°$ (−13.8 kcal mol^{-1}), $\Delta S°$ (−39.6 cal mol^{-1} K^{-1}), and $\Delta G°_{298}$ (−2.0 kcal mol^{-1}) were calculated for the insertion of CO_2 into the Sn−OtBu bond. As there was no measurable amount of isopropoxide

(27) Fogg, P. G. T.; Gerrard, W. In *Solubility of Gases in Liquids*; John Wiley & Sons: Chichester, England, 1991, p 249.

Scheme 2. Reaction of Alkoxides **2a**−**2c** with CO_2 to Form Carbonates **5a**−**5c** and the Various Equilibria Involved

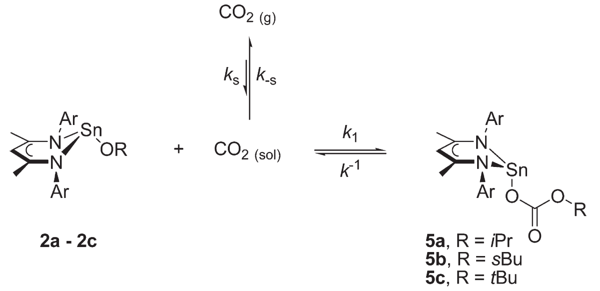

Table 4. Ratio of Alkoxide **2** to Carbonate **5**, K_{eq} $\Delta G°_{313}$ (kcal mol^{-1}), and Relative Time to Equilibrium (t_{equil}) for the Equilibrium between **2**/CO_2 and **5**[a]

	2: **5**	K_{eq}	$\Delta G°_{313}$	(t_{equil})
^{i}Pr (**2a**/**5a**)	7.6:92.4	191	−3.27	3 h
^{s}Bu (**2b**/**5b**)	11.1:88.9	178	−3.22	1 d
^{t}Bu (**2c**/**5c**)	45.4:54.6	20	−1.88	3 d

[a] All measurements were performed in C_6D_6 at 313 K using 36.4 mM alkoxide in a sealed NMR tube with a 50 cm^3 head-space (to maintain a steady CO_2 concentration). The calculated CO_2 concentration at this temperature is 0.091 M.

or *sec*-butoxide at room temperature, the $\Delta H°$ and $\Delta S°$ was not determined for these latter systems.

Although we were able to flood with carbon dioxide to obtain accurate equilibrium measurements, determination of the reaction rate using NMR spectroscopy was impossible because of limited ability to mix the solution, resulting in diffusion of carbon dioxide to be rate influencing. We were able to qualitatively gauge the reaction rate; for the isopropoxide system, equilibrium was established after 3 h at 313K, for the *sec*-butoxide system, equilibrium was established after 1 d at 313 K, and for the *tert*-butoxide system, equilibria was established after 3 d at 313K; however, all reactions proceeded faster when the NMR tube was shaken. Unfortunately, UV−vis spectroscopic measurements gave unreliable results, thus thwarting our attempts to examine the relative rates in greater detail.

Nonafluoro-*tert*-butoxide Tin Complex. The nonafluoro-*tert*-butoxide tin complex **2d** was synthesized in order to gauge the role of steric and electronic factors in the reactivity trends of the tin alkoxides **2a**−**2c**. The X-ray crystal structure was determined for **2d**, and revealed a significantly shorter O−C31 bond length when compared to the per-protio *tert*-butoxide analogue **2c**, presumably due to the electronic withdrawing nature of the fluoroalkyl groups (Figure 3). The Sn−O bond length of 2.110(2) Å is significantly longer than **2c** (2.0179(16) Å). This can be attributed to the increased ionic nature of the Sn−O bond, which is also reflected in the shortened Sn−N bond lengths (average 2.1837 Å for **2d** versus average 2.2058 Å for **2c**). Potential long-range Sn···F interaction is observed between Sn and F1 (3.204 Å), F2 (3.353 Å) and F9 (3.433 Å) as all of these distances are shorter than the sum of the Sn−F radii of 3.64 Å, consistent with other fluoroalkoxide complexes.[28,29]

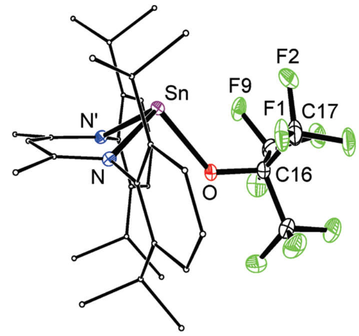

Figure 3. ORTEP diagram of (BDI)SnO^{t}Bu^F **2d** (fluorine atoms in green) with H atom omitted and BDI aryl groups C atoms minimized for clarity; ellipsoid probability shown at 30%.

Treatment of (BDI)SnO^{t}Bu^F **2d** with methyl triflate produces an intractable mixture of products; no evidence for either (BDI)Sn-OTf or MeOC(CF_3)$_3$ was found. Addition of maleic anhydride to **2d** leads to the protonated ligand LH and no isolable tin containing species. In sharp contrast to the perprotonated alkoxides **2a**−**2c**, perfluoro **2d** does not react with carbon dioxide.

Computational Studies. Density Functional Theory (DFT) studies were performed to further understand the influence of the alkyl group on both the thermodynamics and kinetics for the formation of tin alkylcarbonates from the reaction of tin alkoxides with carbon dioxide. Geometry optimization and single point energy calculations were performed on tin alkoxides **2a**, **2b**, **2c**, and **2d** and the corresponding alkylcarbonates **5a**, **5b**, **5c**, and **5d** using a B3LYP/Lanl2dz/3-21 g level of theory for the geometry optimization of the entire molecule followed by a single point energy calculation using a larger basis set (see Experimental Section).[30] The geometry optimization for the alkoxide complexes (**2a**, **2b**, **2c**, and **2d**) are in good agreement with the experimental results, although the N−Sn−O bond angles are overestimated by 5 − 7% for the nonfluorinated alkoxide complexes **2a**−**2c** (see Supporting Information). The ΔG°_{298} for the insertion of carbon dioxide into the tin alkoxide was calculated to be closer to neutrality than our experimental results, with a positive ΔG°_{298} for the *sec*-butyl and *tert*-butyl systems and a negative ΔG°_{298} for the isopropyl system. However, the trends in reactivity of the different alkyl groups correspond to what we observe; that is, the ΔG°_{298} was more positive for the *tert*-butoxide system and the least positive for the isopropoxide system.

An abbreviated molecule in which the *N*-aryl groups, as well as the backbone methyl groups, are replaced with protons, [CH{CHCNH}$_2$]$^-$ (L*) was used to give further mechanistic insight into the insertion of carbon dioxide into the tin−oxygen bond.[31] This smaller ligand was utilized in looking for transition states in the reaction pathway and, because of the minimal steric influence of this ligand, providing information about the different electronic contributions from each of the different alkoxide substituents. The reaction profile for the conversion of L*SnO^{i}Pr to the corresponding metallo-alkylcarbonate

(28) Reisinger, A.; Trapp, N.; Krossing, I.; et al. *Organometallics* **2007**, *26*, 2096.
(29) Samuels, J. A.; Lobkovsky, E. B.; Streib, W. E.; Folting, K.; Huffman, J. C.; Zwanziger, J. W.; Caulton, K. G. *J. Am. Chem. Soc.* **1993**, *115*, 5093.
(30) Frisch, M. J. et al. et. al. *Gaussian 03*, revision C.02; Gaussian, Inc.: Wallingford, CT, 2004.
(31) Liu, C.; Munjanja, L.; Cundari, T. R.; Wilson, A. K. *J. Phys. Chem. A* **2010**, *114*, 6207.

Table 5. Calculated Thermodynamic (kcal mol^{-1}) and Kinetic (s^{-1}) Parameters at the B3LYP/[4333111/433111/43]/6-31g(d,p) Level of Theory, for the Transformation of (BDI)SnOR to (BDI)SnO(CO_2)R and L*SnOR to L*SnO(CO_2)R

	L = BDI			L* = [CH {CHCNH}$_2$]					
	$\Delta G°$	$\Delta H°$	$\Delta E°$	$\Delta G°$	$\Delta H°$	$\Delta E°$	$\Delta G^‡$	$\Delta H^‡$	$\Delta E^‡$
^{i}Pr	−0.0	−9.7	−9.5	−4.0	+7.0	−13.7	+10.4	+0.8	+0.8
^{s}Bu	+0.5	−10.8	−10.2	−2.9	−12.4	−12.4	+12.4	2.5	+2.5
^{t}Bu	+1.1	−10.0	−9.4	−0.3	−12.0	−11.3	+15.6	3.6	+4.2
^{t}Bu^F	+17.5	+7.0	+7.6	+20.4	9.4	+10.1	NA	NA	NA

L*SnOCO$_2$^{i}Pr is shown in Figure 4, and includes the relative energies of the reactants (**Alk-a**), transition state (**TS-a**), intermediate (**INT-a**) and carbonate (**Carb-a**).

Because of the low reactivity of the tin alkoxides with aliphatic electrophiles, we initially examined a nonnucleophilic pathway in which carbon dioxide coordinates directly to the metal center, and insertion of carbon dioxide into the Sn−O bond would follow. Although rare, coordination of carbon dioxide to coordinatively unsaturated metal centers has been observed, most commonly in an η^2-fashion,[32−35] but end-on coordination has also been found.[36] A high energy transition state (**TS^{NP}**, $\Delta G^‡ = 56.6$ kcal mol^{-1}) was located in which carbon dioxide coordinates in an η^2-fashion to the tin center of isoproxide **Alk-a**. This interaction involves the tin 5*s* lone pair binding to an antibonding orbital located on the carbon dioxide molecule. As a result, there is a predictable decrease in electron density at the metal center and an increase in electron density at the carbon atom (see Figure 5 for Mulliken charge distribution). The C−O2 bond length is significantly longer than experimentally derived η^2-CO_2 complexes,[32−35] opening up the possibility that this transition state structure is best described as a metallacycle in which there has been an oxidative addition of C=O to the metal center, generating a tin(IV) complex.

Because of both the high-energy nature of this structure and our inability to find a pathway from **TS^{NP}** to the corresponding carbonate (**Carb-a**), this transition state was deemed nonproductive. An alternative and more energetically accessible transition state was found arising from an interaction between the oxygen lone pair (HOMO −1) on the tin alkoxide and the LUMO of CO_2 (**TS-a**, $\Delta G^‡ =$ 16.6 kcal mol^{-1}). This four-membered transition state involves formation of a new C−O1 bond, weakening of the C=O2 double bond, formation of a new Sn−O2 bond and a weakening of the Sn−O1 bond. The C···O1 interaction of 1.869 Å results in a slight C=O bond elongation of 0.017 Å (C−O2) and 0.039 Å (C−O3), a decrease in the O2−C−O3 bond angle to 151° and an elongation of the Sn−O bond by 0.121 Å. The Wiberg bond index (WBI) of the formation C−O1 bond is 0.33, whereas the WBI of the Sn−O1 bond has decreased by 0.19− 0.37, indicating that although there has been minimal geometric change within the Sn−O1 bond, there has been significant weakening.

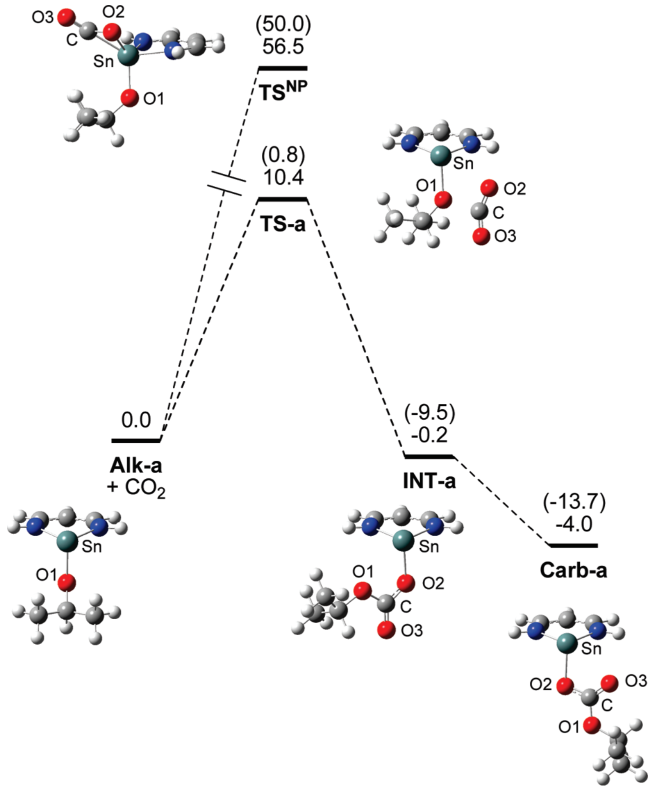

Figure 4. Gibbs free energy diagram (kcal mol^{-1}) and drawings for the reaction of L*SnO^{i}Pr with CO_2 at the B3LYP level. Electronic energy values are given in parentheses.

The Sn···O2 interaction of 2.733 Å is well within their combined Van der Waal radii of 3.69 Å and is shorter than the long-range interaction observed for maleate **4**. Although the WBI of 0.09 shows very little direct electronic interaction, the Mulliken population analysis shows there is a build-up of negative charge on O2 (−0.45 for the O2 atom in the **TS-a** compared to −0.33 fro the free carbon dioxide). Taken with the increase of positive charge from +0.71 to +0.83 of the tin atom, there could be an electrostatic Sn−O2 interaction that has not been accounted for in our calculations. Once **TS-a** is formed, a smooth transition to the metallo-alkylcarbonate intermediate, **INT-a**, is observed and no intermediates between **TS-a** and **INT-a** were calculated during an Intrinsic Reaction Coordinate (IRC) calculations.

INT-a possesses a formal Sn−O2 bond, the Sn···O1 distance is 2.913 Å, which is shorter than the sum of the combined van der Waals radii (WBI = 0.05) and no interaction exists between Sn and O3. A similar intermediate has also been observed by Wakamatsu and Otera.[37] After formation of **INT-a**, the Sn−O2 bond rotates such that the bulky alkyl group projects away from the metal center and a new Sn···O3 interaction is formed (2.728 Å, WBI = 0.11). The final product, **Carb-a**, is analogous to that reported for the lead isopropoxide system, in which there is a long distance Pb···O3 interaction.

The corresponding calculations were performed on the other alkoxide complexes, *sec*-butoxide **Alk-b**, *tert*-butoxide **Alk-c** and nonafluoro-*tert*-butoxide **Alk-d**, and their corresponding metallo-alkylcarbonates **Carb-b-d**. The $\Delta G°_{298}$

(32) Hirano, M.; Akita, M.; Tani, K.; Kumagai, K.; Kasuga, N. C.; Fukuoka, A.; Komiya, S. *Organometallics* **1997**, *16*, 4206.
(33) Fu, P. F.; Khan, M. A.; Nicholas, K. M. *J. Organomet. Chem.* **1996**, *506*, 49.
(34) Alvarez, R.; Carmona, E.; Marin, J. M.; Poveda, M. L.; Gutierrezpuebla, E.; Monge, A. *J. Am. Chem. Soc.* **1986**, *108*, 2286.
(35) Gambarotta, S.; Strologo, S.; Floriani, C.; Chiesivilla, A.; Guastini, C. *J. Am. Chem. Soc.* **1985**, *107*, 6278.
(36) Castro-Rodriguez, I.; Nakai, H.; Zakharov, L. N.; Rheingold, A. L.; Meyer, K. *Science* **2004**, *305*, 1757.
(37) Wakamatsu, K.; Orita, A.; Otera, J. *Organometallics* **2010**, *29*, 1290.

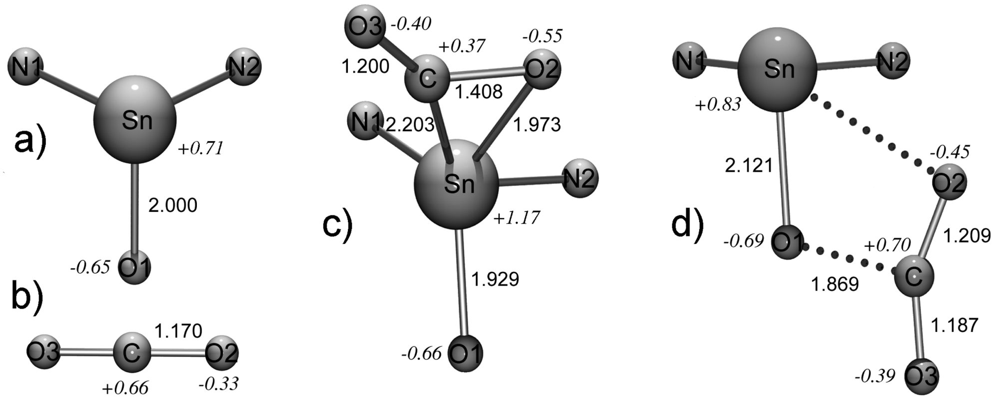

Figure 5. Optimized geometries and Mulliken charges for (a) **Alk-a**, (b) $\mathbf{CO_2}$, (c) $\mathbf{TS^{NP}}$, and (d) **TS-a**. Only Sn, N, O, and carbon dioxide atoms of the model complex are shown for clarity.

and $\Delta E°$ for the reactions follow the same trends as the larger systems (Table 4); that is, the isopropyl system as the most negative $\Delta G°_{298}$ and $\Delta E°$, followed by the *sec*-butyl and *tert*-butyl system, respectively. The fluorinated system has a significantly positive $\Delta G°_{298}$ and $\Delta E°$, which is in agreement with our experimental results in with the nonafluoro-*tert*-butoxide **2d** doe not react with carbon dioxide. A transition state was located for the *sec*-butyl system (**TS-b**) and the *tert*-butyl system (**TS-c**); however, no transition state was found for the fluorinate derivative (**TS-d**).

Discussion

The tin(II) alkoxide complexes **2a**−**2d** do not exhibit the standard reactivity as their transition metal counterparts; their lack of reactivity with methyl iodide indicates that the oxygen atom is essentially non-nucleophilic toward anything but very strong electrophiles such as methyl triflate. The notable difference in reactivity *between* the alkoxides **2a**−**2c** might be attributable to steric effects; the combination of the bulky β-diketiminate ligand as well as the *tert*-butoxide ligand of **2c** results in a more hindered approach to the oxygen atom than the corresponding isopropoxide system **2a**. However, there is also a compelling electronic argument as the reactivity trend mirrors the relative basicity of the alkoxide moieties; that is, the greater the basicity, or the greater the pK_a of the conjugate acid, the more reactive the alkoxide.[38,39] Because the reaction between the tin alkoxides and methyl triflate is irreversible, it is impossible to differentiate between steric and electronic arguments based solely on this reaction.

The activation of carbon dioxide by a seemingly non-nucleophilic metal alkoxide complex is counterintuitive. It has previously been show that the nucleophilicity of the alkoxide ligand drives insertion reactions.[1] Studies on rhenium alkoxide and aryloxide complexes, (*fac*$(CO)_3(PMe_3)_2$ReOR, revealed that only the alkoxide (R = Me) reacts with carbon dioxide, yet both alkoxide and aryloxide (R = 4-MeC_6H_4) react with carbon disulfide. Darensbourg observed that (*fac*)-$(CO)_3$(dppe)MnOMe reacts more readily with carbon dioxide than $(CO)_3$(dppe)$MnOCH_2CF_3$, a less nucleophilic alkoxide ligand.[9] The mechanism of carbon dioxide insertion in this case was postulated to proceed via a four-membered transition state, similar to what we observed in our calculations and have been proposed by others.[3,9,13,37]

A few transition metal systems have been reported to react with both methyl iodide and carbon dioxide, unfortunately most reports have been vague on the reaction conditions.[40,41] Vahrenkamp's pyrazolylborate-zinc methoxide complex, $(Tp^{Ph,Me})$ZnOMe, reacts readily with methyl iodide but very slowly with carbon dioxide, in sharp contrast to our results.[11] The former reaction is attributed to the nucleophilicity of the zinc-alkoxide. Thus, it can not only be the nucleophilicity of the alkoxide ligand that is governing the reactivity of alkoxides with carbon dioxide (vide infra). Interestingly, trispyrazolborate zinc *hydroxides* do react readily and reversibly with carbon dioxide,[42,43] although this could be because of hydrogen-bonding effects.

Another intriguing aspect about our results is the strong dependence on both the reaction rate as well as final equilibrium on minor variations of the alkyl group on the alkoxide ligand. This it true both with the tin and lead systems. The insertion of carbon dioxide into the Sn−O bond to generate metallo-alkylcarbonates is measurably reversible; as such, by using the equilibrium studies as well as the computational studies on the transition state, the factor governing the influence of the alkyl group can be examined. In order to normalize the different alkyl systems onto one scale, a "zero-point" was set by assuming that the alkyl group has a greater inductive influence on the ground state energy of the alkoxide **Alk** than the metallo-alkylcarbonate **Carb**. Electronic influences of the different alkyl groups are apparent upon considering the pK_a's of aliphatic alcohols;[39,44] however, these electronic influences are not apparent upon considering either the bond dissociation energies (BDE's) or pK_a's of the corresponding carboxylic acids,[45] and only minor variations within experimental error of each other are observed in the BDE's of the corresponding alcohols. As such, the relative energies of our metallo-alkylcarbonates **Carb-a-c** can be set to "zero" and all other energies can be compared to these metallo-alkylcarbonates (Figure 6).

(38) Bryndza, H. E.; Fong, L. K.; Paciello, R. A.; Tam, W.; Bercaw, J. E. *J. Am. Chem. Soc.* **1987**, *109*, 1444.
(39) Brauman, J. I.; Blair, L. K. *J. Am. Chem. Soc.* **1970**, *92*, 5986.
(40) Park, S.; Rheingold, A. L.; Roundhill, D. M. *Organometallics* **1991**, *10*, 615.
(41) Bryndza, H. E.; Tam, W. *Chem. Rev.* **1988**, *88*, 1163.
(42) Ruf, M.; Vahrenkamp, H. *Inorg. Chem.* **1996**, *35*, 6571.
(43) Looney, A.; Han, R.; McNeill, K.; Parkin, G. *J. Am. Chem. Soc.* **1993**, *115*, 4690.
(44) Olmstead, W. M.; Margolin, Z.; Bordwell, F. G. *J. Org. Chem.* **1980**, *45*, 3295.
(45) Blanksby, S. J.; Ellison, G. B. *Acc. Chem. Res.* **2003**, *36*, 255.

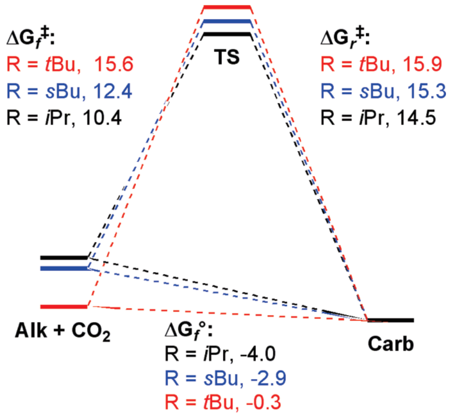

Figure 6. Energy diagram for the interconversion of **Alk** + CO_2 and **Carb** via transition state **TS**. Energies are reported in kcal mol^{-1}. $\Delta G_f°$ is the change in Gibbs free energy in the forward sense, $\Delta G_f^‡$ is the activation energy in the forward reaction and $\Delta G_r^‡$ is the activation energy for the reverse reaction.

In the isopropoxide system, the conversion from **Alk-a** to **Carb-a** has a relatively low activation barrier and the overall reaction is thermodynamically favored. In contrast, the conversion from **Alk-c-** to **Carb-c** in the *tert*-butoxide system is almost thermodynamically neutral and a significantly higher activation barrier is found. Steric arguments cannot fully explain the thermodynamic differences, these must be a consequence of the relative bond dissociation energies (BDE's) of the Sn-OR bond. If it is assumed that the Sn−O2 BDE for the metallo-alkylcarbonates is relatively similar due to reasons previously described, then the BDE of the Sn−O^{t}Bu bond is greater than that of the Sn−O^{s}Bu bond and the Sn−O^{i}Pr bond is the weakest of the three. Thus, in the forward sense of the reaction, in order to achieve the transition state, the energy required is greater for the *tert*-butoxide system than the isopropoxide system, thus the Sn−O bond of isopropoxide **Alk-a** must be weaker than the Sn−O bond of *tert*-butoxide **Alk-c**. Although the activation barriers to the reverse reaction follow a similar pattern in which the *tert*-butoxide system has a greater activation barrier than the isopropoxide system, the difference is not as great and can be attributed to a combination of steric arguments and the differences in the O1−C bond strengths. For the real molecule, (BDI)SnOR, the reverse reaction should be more affected by the sterics of the alkoxide group due to the interactions of both the BDI *N*-aryl groups and the alkoxide.

Although nonafluoro-*tert*-butoxide tin complex **2d** is nonreactive with carbon dioxide, the calculations show that the postulated carbon dioxide insertion product is significantly higher in energy than just **2d** and carbon dioxide. However, a direct comparison with the other alkoxide complexes **2a**−**2c** cannot be made because, in contrast to the nonfluorinated derivatives, the pK_a of the fluorinated alcohol and carboxylic acid are heavily influenced by the nearby fluorine atoms.[46]

The contrast between the reactivity of group 14 alkoxides and Vahrenkamp's zinc alkoxides is striking and reveals that it is not just the nucleophilicity of the alkoxide ligand that determines its reactivity with carbon dioxide. Although there are too many variables between group 14 alkoxides and (Tp^{Ph,Me})ZnOMe to make a meaningful comparison, the tin and lead systems can be compared. The higher reactivity of the lead system can be attributed to a combination of a more polarized and weaker Pb−O bond, resulting in a more nucleophilic alkoxide ligand and a more Lewis acidic lead metal center, which forms a more stable four-membered transition state due to a greater interaction with the CO_2 oxygen atom. The tin system suffers both from a stronger Sn−O bond, low nucleophilicity of the alkoxide ligand, as well as a smaller Lewis acidity of the metal center, thus requiring a higher activation barrier in its reaction with carbon dioxide.

Conclusions

Tin alkoxide complexes **2** are weakly nucleophilic species that only react with highly reactive aliphatic electrophiles; however, these complexes do react reversibly with carbon dioxide, due to a combination of a weakly nucleophilic alkoxide ligand and a Lewis acidic metal center that can help support the four-membered transition state. The rate of reaction as well as the relative equilibrium between reactants and products is dependent upon the alkoxide ligand. The isopropoxide complex **2a** reacts with carbon dioxide faster than the bulkier *tert*-butoxide complex **2c**, and the former reaction has a greater equilibrium constant than the latter. Although the sterics of the alkoxide ligand might play a role in these results, computational studies have shown that there is a significant electronic contribution to both the activation barrier as well as the established equilibrium. If it is assumed that the Sn−O BDE of the metallo-alkylcarbonate **5** complexes are less influenced by the alkyl substituent than the Sn−O BDE of the alkoxide complexes **2**, then a relative ordering of the Sn−O BDE can be made, with the *tert*-butoxide complex **2c** possessing the strongest Sn−O BDE, and the isopropoxide complex **2a** possessing the weakest Sn−O BDE. Interestingly, the *tert*-butoxide complex **2c** has the longest Sn−O bond and the isopropoxide complex **2a** has the shortest Sn−O bond.

Experimental Section

General. All manipulations were carried out under an atmosphere of dry nitrogen using standard Schlenk techniques or in an inert-atmosphere glovebox. Solvents were dried from the appropriate drying agent, distilled, degassed, and stored over 4 Å sieves. (BDI)SnCl and (BDI)SnO^{i}Pr were prepared according to the literature.[15,23] Potassium alkoxide salts were prepared by the slow addition of the relevant alcohol (dried and distilled) to a suspension of potassium hydride, except NaO^{t}Bu^F that was prepared by the treatment of a water solution of $(CF_3)_3COH$ with 1eq of NaOH and dried overnight under vacuum over P_2O_5. Methyl trifluoromethanesulfonate was freshly dried and distilled before use. Carbon dioxide was used as received (Union Carbide, 99.999%), and $^{13}CO_2$ was 99 atom %. ^{1}H, ^{13}C and ^{119}Sn NMR spectra were recorded on a Varian 400 MHz or Varian 500 MHz spectrometer. ^{1}H and ^{13}C NMR spectroscopy chemical shifts are given relative to residual solvent peaks and ^{119}Sn was externally referenced to $SnMe_4$. The UV spectra were recorded in Varian Cary 50 UV−vis spectrophotometer. The data for X-ray structures were collected at 173 K on a Nonius KappaCCD diffractometer, k(Mo−Kα) = 0.71073 Å and refined using the *SHELXL-97* software package.[47]

[CH{(CH$_3$)CN-2,6-^{i}Pr$_2$C$_6$H$_3$}$_2$SnO^{i}Pr] (2a). (BDI)SnOiPr was prepared following literature procedures. The ^{1}H and ^{13}C NMR spectra were identical to the ones reported earlier.[15]

(46) Arnett, E. M.; Venkatasubramaniam, K. G. *J. Org. Chem.* **1983**, *48*, 1569.

(47) Sheldrick, G. M. *SHELXL-97, Program for the Refinement of Crystal Structures*; University of Göttingen: Göttingen, Germany, 1997.

UV−vis (benzene): λ_{max} (ε, L mol^{-1} cm^{-1}) 366 nm (11000). IR (CCl_4, ν/cm^{-1}): 2964 (s), 2925 (s), 1464 (s), 1430, 1359, 1315 (s), 1170, 1101 (s).

[CH{(CH$_3$)CN-2,6-^{i}Pr$_2$C$_6$H$_3$}$_2$SnO^{s}Bu] (2b). A suspension of KO^{s}Bu (98 mg, 0.87 mmol) in THF (5 mL) was added to a solution of (BDI)SnCl (0.50 g, 0.87 mmol) in THF (5 mL) at room temperature, and the reaction mixture was stirred for 3 d. The solvent was removed under vacuum, the yellow crude product was extracted with toluene and the solution was filtered through Celite. Removal of the volatiles and recrystallization from pentane overnight afforded yellow crystals of (BDI)SnO^{s}Bu (0.42 g, 80%). ^{1}H NMR (400 MHz, C_6D_6, 303 K): δ 7.22 (d, J = 7.6, 2H, ArH), 7.14 (t, J = 7.6, 2H, ArH), 7.07 (d, J = 7.7, 2H, ArH), 4.71 (s, 1H, $\gamma\sigma$-CH), 3.81 (m, 3H, CHMe$_2$ + OCH(Me)Et), 3.22 (m, 2H, CHMe$_2$), 1.55 (s, 3H, NCMe), 1.54 (s, 3H, NCMe), 1.50 (d, J = 6.1, 3H, CHMe), 1.48 (d, J = 6.1, 3H, CHMe), 1.25 (d, J = 6.8, 6H, CHMe), 1.19 (d, J = 6.9, 6H, CHMe), 1.11 (d, J = 6.8, 6H, CHMe), 0.75 (d, J = 6.0, 3H, OCH(Me)Et, 0.46 (t, J = 7.4, OCH(Me)CH$_2$$Me$). ^{13}C{^{1}H} NMR (500 MHz, C_6D_6, 303 K): δ 164.6 (NCMe), 144.9 ($ipso$-C), 142.6 (o-C), 141.1 (o-C), 126.2 (p-C), 124.3 (m-C), 123.8 (m-C), 96.3 (γ-CH), 70.7 (OCH(Me)Et), 34.9 (OCH(Me)CH$_2$Me), 28.2 (NCMe), 28.1 (NCMe), 26.6 (CHMe), 26.0 (CHMe), 24.6 (CHMe), 24.4 (CHMe), 24.3 (CHMe), 24.2 (CHMe), 23.1 (OCH(Me)Et), 10.3 (OCH(Me)CH$_2$$Me$). ^{119}Sn NMR (400 MHz, C_6D_6, 303 K): δ −181.5. UV−vis (benzene): λ_{max} (ε, L mol^{-1} cm^{-1}) 366 nm (12000). IR (Nujol, ν/cm^{-1}): 1554 (s), 1518 (s), 1260 (s), 1098, 1018 (s), 795 (s). IR (CCl_4, ν/cm^{-1}): 2966 (s), 2925 (s), 1463 (s), 1423, 1314 (s), 1172, 1104. Anal. Calcd for $C_{33}H_{50}N_2OSn$: C, 65.03; H, 8.27; N, 4.60. Found: C, 64.96; H, 8.23; N, 4.57.

[CH{(CH$_3$)CN-2,6-^{i}Pr$_2$C$_6$H$_3$}$_2$SnO^{t}Bu] (2c). Yellow crystals of (BDI)SnO^{t}Bu can be obtained in good yield (76%) using a similar methodology as used in the preparation of (BDI)SnO^{s}Bu **2b**. ^{1}H NMR (400 MHz, C_6D_6, 303 K): δ 7.18 (d, J = 7.6, 2H, ArH), 7.14−7.06 (m, J = 7.6, 2H, ArH), 7.03 (d, J = 7.6, 2H, ArH), 4.61 (s, 1H, γ-CH), 3.86−3.71 (m, 2H, CHMe$_2$), 3.29−3.14 (m, 2H, CHMe$_2$), 1.54 (s, 6H, NCMe), 1.53 (d, J = 6.9, 6H, CHMe), 1.28 (d, J = 6.8, 6H, CHMe), 1.17 (d, J = 6.9, 6H, CHMe), 1.12 (d, J = 6.8, 6H, CHMe), 0.86 (s, 9H, OC(Me)$_3$). ^{13}C{^{1}H} NMR (400 MHz, C_6D_6, 303 K): δ 169.4 (NCMe), 165.0 (NCMe), 144.9 ($ipso$-C), 142.6 (o-C), 140.9 (o-C), 126.1 (p-C), 123.9 (m-C), 123.8 (m-C), 95.5 (γ-CH), 69.4 (OC(Me)$_3$), 34.9 (OC(Me)$_3$), 28.2 (NCMe), 28.2 (NCMe), 26.1 (CHMe), 24.4 (CHMe), 24.3 (CHMe), 24.2 (CHMe), 23.0 (CHMe). ^{119}Sn NMR (400 MHz, C_6D_6, 303 K): δ −149.1. UV−vis (benzene): λ_{max} (ε, L mol^{-1} cm^{-1}) 365 nm (13000). IR (Nujol, ν/cm^{-1}): 1555 (s), 1261 (s), 1093, 1018 (s), 939 (s), 796 (s). IR (CCl_4, ν/cm^{-1}): 2965 (s), 2927 (s), 1463 (s), 1424, 1361, 1171 (w). Anal. Calcd for $C_{33}H_{50}N_2OSn$: C, 65.03; H, 8.27; N, 4.60. Found: C, 64.97; H, 8.32; N, 4.55.

[CH{(CH$_3$)CN-2,6-^{i}Pr$_2$C$_6$H$_3$}$_2$SnOC(CF$_3$)$_3$] (2d). A solution of NaO^{t}Bu^F (0.14 g, 0.55 mmol) in THF (5 mL) was added to a solution of (BDI)SnCl (0.31 g, 0.55 mmol) in THF (5 mL) at room temperature, and the reaction mixture was stirred for 3 d. The solvent was removed under vacuum, the yellow crude product was extracted with toluene and the solution was filtered through Celite. The volatiles were removed and the yellow/green solid was washed with pentane. Recrystallization from THF overnight afforded green crystals of (BDI)SnO^{t}Bu^F (0.29 g, 69%). ^{1}H NMR (400 MHz, C_6D_6, 303 K): δ 7.16 (d, J = 7.6, 2H, ArH), 7.09 (d, J = 7.7, 2H, ArH), 7.03 (d, J = 7.7, 2H, ArH), 4.55 (s, 1H, γ-CH), 3.80 − 3.34 (m, 2H, CHMe$_2$), 3.16 − 2.76 (m, 2H, CHMe$_2$), 1.45 (d, J = 5.7, 6H, CHMe), 1.44 (s, 6H, NCMe), 1.23 (d, J = 6.8, 6H, CHMe), 1.10 (d, J = 6.7, 6H, CHMe), 1.09 (d, J = 6.5, 6H, CHMe). ^{13}C{^{1}H} NMR (500 MHz, C_6D_6, 303 K): δ 166.0 (NCMe), 143.8 ($ipso$-C), 142.2 (o-C), 139.7 (o-C), 127.5 (p-C), 126.8 (m-C), 124.3 (m-C), 96.4 (γ-CH), 67.4 (OC(CF$_3$)$_3$), 28.6 (OC(CF$_3$)$_3$), 28.3 (NCMe), 25.4 (CHMe), 24.6 (CHMe), 24.3 (CHMe), 23.0 (CHMe), 23.0 (CHMe). ^{19}F NMR (400 MHz, C_6D_6, 303 K): δ −73.0. ^{119}Sn NMR (400 MHz, C_6D_6, 303 K): δ −256.3. UV−vis (benzene): λ_{max} (ε, L mol^{-1} cm^{-1}) 320 nm (22000). IR (Nujol, ν/cm^{-1}): 2024, 1945, 1548, 1518, 1319, 1262 (s), 1233 (s), 1167 (s), 1017, 966 (s), 795. Anal. Calcd for $C_{33}H_{41}F_9N_2OSn$: C, 51.38; H, 5.36; N, 3.63. Found: C, 51.41 ; H, 5.30; N, 3.64.

[CH{(CH$_3$)CN-2,6-^{i}Pr$_2$C$_6$H$_3$}$_2$SnO(CO)C$_2$H$_2$CO$_2$^{i}Pr] (4). A solid mixture of (BDI)SnO^{i}Pr (250 mg, 0.41 mmol) and maleic anhydride (40 mg, 0.41 mmol) was dissolved in toluene (10 mL) and stirred for 2 h, affording an orange solution. After evaporation of the solvent, the residue was dissolved in the minimum amount of hexane. Storage at −32 °C for 3 days afforded deep red crystals of (BDI)Sn(Ma)^{i}Pr (248 mg, 87%). ^{1}H NMR (400 MHz, C_6D_6, 303 K): δ 7.21 − 6.93 (m, 6H, ArH), 5.96 (d, J = 11.9 Hz, 1H, COCHCHCO$_2$), 5.83 (d, J = 12.0 Hz, 1H, COCHCHCO$_2$), 5.09 (sept, 6.0 Hz, 1H, CO$_2$CHMe$_2$), 4.91 (s, 1H, γ-CH), 3.62 (sept, J = 6.7 Hz, 2H, CHMe$_2$), 3.04 (sept, J = 6.7 Hz, 2H, CHMe$_2$), 1.59 (s, 6H, NCMe), 1.37 (d, J = 6.6 Hz, 6H, CHMe_2), 1.27 (d, J = 6.7 Hz, 6H, CHMe_2), 1.12 (d, J = 6.8 Hz, 6H, CHMe_2), 1.07 (d, J = 6.2 Hz, 6H, CHMe_2), 1.04 (d, J = 6.8 Hz, 6H, CHMe_2). ^{13}C{^{1}H} NMR (400 MHz, C_6D_6, 303 K): δ 170.0 (SnOCO), 169.3 (CO$_2$^{i}Pr), 165.40 (NCMe), 145.31 ($ipso$-C), 142.43 (o-C), 141.27 (o-C), 131.0 (CH=CH), 130.0 (CH=CH), 127.1 (p-C), 124.8 (m-C), 123.7 (m-C), 99.8 (γ-CH), 67.5 (CO$_2$CHMe$_2$), 28.7 (NCMe), 27.7 (NCMe), 26.4 (CHMe), 24.6 (CHMe), 24.1 (CHMe), 23.60 (CHMe), 21.4 (CHMe). ^{119}Sn NMR (400 MHz, C_6D_6, 303 K): δ −374.2. IR (Nujol, v/cm^{-1}): 1735 (s), 1600, 1552, 1524, 1261 (s), 1211, 1172, 1102 (s), 1019 (s), 797(s). Anal. Calcd for $C_{36}H_{50}N_2O_4Sn$: C, 62.35; H, 7.27; N, 4.04. Found: C, 62.39; H, 7.15; N, 3.94.

Generation of Metallocarbonates 5a, 5b, and 5c: General Procedure. (BDI)SnO^{i}Pr (8.5 mg, 0.014 mmol) was dissolved in C_6D_6 (400 μL) in an NMR tube sealed with a Young's tap. The NMR tube was submerged in a dry ice/ethanol bath, the gas inside the NMR tube was evacuated and CO_2 was introduced at a pressure of 1 atm. A pale yellow solution mixture was observed, the reaction mixture was kept at room temperature for 48 h and was monitored by ^{1}H NMR spectroscopy. To generate samples for IR spectroscopy, a similar procedure was followed using CCl_4 as solvent.

[CH{(CH$_3$)CN-2,6-^{i}Pr$_2$C$_6$H$_3$}$_2$SnO(CO$_2$)^{i}Pr] (5a). ^{1}H NMR (400 MHz, C_6D_6, 303 K): δ 7.27−6.95 (m, 6H, ArH), 4.95 (s, 1H, γ-CH), 4.89 (dq, J = 6.2, 1H, CO$_2$CHMe$_2$), 3.71 (hept, J = 6.7, 2H, CHMe$_2$), 3.07 (hept, 2H, J = 6.9, CHMe$_2$), 1.59 (s, 6H, NCMe), 1.44 (d, J = 6.7, 6H, CHMe), 1.22 (d, J = 6.8, 6H, CHMe), 1.18 (d, J = 6.3, 6H, CHMe), 1.16 (d, J = 7.0, 6H, CHMe), 1.06 (d, J = 6.8, 6H, CO$_2$CHMe). ^{13}C{^{1}H} NMR (400 MHz, C_6D_6, 303 K): δ 165.2 (NCMe), 158.7 (OCO$_2$), 145.4 ($ipso$-C), 142.5 (o-C), 141.3 (o-C), 127.1 (p-C), 124.7 (m-C), 123.6 (m-C), 99.7 (γ-CH), 68.5 (OCO$_2$-CHMe$_2$), 28.7 (OCO$_2$CHMe_2), 27.7 (NCMe), 26.0 (NCMe), 24.5 (CHMe), 24.1 (CHMe), 23.9 (CHMe), 23.5 (CHMe), 22.0 (CHMe). ^{119}Sn NMR (400 MHz, C_6D_6, 303 K): δ −379.7. UV−vis (benzene): λ_{max} 321 nm. IR (CCl_4, ν/cm^{-1}): 3963, 2963 (s), 2927, 2871, 2339 (s), 1718 (w), 1621, 1463, 1437, 1385, 1318.

[CH{(CH$_3$)CN-2,6-^{i}Pr$_2$C$_6$H$_3$}$_2$SnO(CO$_2$)^{s}Bu] (5b). ^{1}H NMR (400 MHz, C_6D_6, 303 K): δ 7.27−7.01 (m, 6H, ArH), 4.93 (s, 1H, γ-CH), 4.72 (m, 1H, CO$_2$CH(Me)Et), 3.72 (hept, J = 6.8, 2H, CHMe$_2$), 3.06 (m, 2H, CHMe$_2$), 1.59 (s, 3H, NCMe), 1.58 (s, 3H, NCMe), 1.47 (d, J = 6.7, 3H, CHMe), 1.45 (d, J = 6.7, 3H, CHMe), 1.27−1.20 (m, 11H, CO$_2$CH(Me)CH_2Me + CO$_2$CH-(Me)CH$_2$Me+ CHMe), 1.16(d, J = 6.9 6H, CHMe), 1.06 (d, J = 6.8, 6H, CHMe), 0.85 (t, J = 7.5, 3H, CO$_2$CH(Me)CH$_2$$Me$). ^{13}C{^{1}H} NMR (400 MHz, C_6D_6, 303 K): δ 167.0 (NCMe), 165.2 (NCMe), 158.8 (OCO$_2$), 145.4 ($ipso$-C), 142.5 (o-C), 141.2 (o-C), 127.0 (p-C), 124.7 (m-C), 123.6 (m-C), 99.8 (γ-CH), 73.3 (OCO$_2$$C$(Me)Et), 29.0 (OCH(Me)$CH_2$Me), 28.7 (NC$Me$), 27.6 (NC$Me$), 26.1 ($C$HMe), 24.5 ($C$HMe), 24.0 (CH$Me$), 23.8 (CH$Me$), 23.4 (CH$Me$), 22.9 (CH$Me$), 19.4 (OCH($Me$)Et), 9.6 (OCH(Me)CH$_2$$Me$). ^{119}Sn NMR (400 MHz, C_6D_6, 303 K): δ − 379.1. UV−vis (benzene): λ_{max} 321 nm. IR (CCl_4, ν/cm^{-1}): 2965 (s), 2928, 2869, 2336 (s), 1720 (w), 1621, 1463, 1437, 1385, 1319, 1101.

[CH{(CH$_3$)CN-2,6-^{i}Pr$_2$C$_6$H$_3$}$_2$SnO(CO$_2$)^{t}Bu] (5c). ^{1}H NMR (400 MHz, C_6D_6, 303 K): δ 7.23−7.06 (m, 6H, Ar*H*), 4.89 (s, 1H, γ-C*H*), 3.68 (hept, J = 6.8, 2H, C*H*Me$_2$), 3.05 (hept, 2H, J = 6.8, C*H*Me$_2$), 1.44 (d, J = 6.7, 6H, CH*Me*), 1.42 (s, 6H, NC*Me*), 1.18 (d, J = 6.8, 6H, CH*Me*), 1.13 (d, J = 6.8, 6H, CH*Me*), 1.02 (d, J = 7.0, 6H, CH*Me*), 0.87 (s, 9H, OC*Me$_3$*). ^{13}C{^{1}H} NMR (400 MHz, C_6D_6, 303 K): δ 167.0 (N*C*Me), 165.3 (N*C*Me), 157.9 (O*C*O$_2$), 145.3 (*ipso-C*), 142.4 (*o-C*), 141.3 (*o-C*), 127.0 (*p-C*), 124.6 (*m-C*), 123.6 (*m-C*), 99.7 (γ-*C*H), 77.1 (O*C*(Me)$_3$), 34.8 (OC(*Me*)$_3$), 28.7 (NC*Me*), 28.0 (NC*Me*), 27.6 (*C*HMe), 26.3 (*C*HMe), 24.4 (CH*Me*), 24.1 (CH*Me*), 23.8 (CH*Me*), 23.4 (CH*Me*). ^{119}Sn NMR (400 MHz, C_6D_6, 303 K): δ −377.4. UV−vis (benzene): λ_{max} 325 nm. IR (CCl_4, ν/cm^{-1}): 2966, 2928, 2870, 2337 (s), 1717 (w), 1621, 1463, 1438, 1386, 1318.

Determination of $t_{1/2}$ for the Reaction of 2a−2c with MeOTf: General Procedure. A sealable NMR tube was charged with 1.7×10^{-5} mol of (BDI)SnOR in 0.25 mL in C_6D_6, 1.1 μL of dichloromethane (1.7×10^{-5} mol) and 1.9 μL of MeOTf (1.7×10^{-5} mol) to give a total volume of 0.25 mL. The NMR tube was then placed in the thermostatted probe (298.1 K) of a Varian 400 MHz spectrometer. The conversion was monitored by ^{1}H NMR spectroscopy. NMR spectra were acquired in 5 min intervals. In order to ensure accurate integration, a 10s delay between 30° pulses was utilized (number of scans = 4, acquisition time = 4). The $t_{1/2}$ was determined by comparing the γ-C*H* signal integration of (BDI)SnOR and (BDI)SnOTf, using the DCM peak as standard.

Equilibrium Studies of the Reaction of 2a−2c with CO$_2$: General Procedure. A 0.45 mL C_6D_6 solution consisting of 1.64×10^{-5} mol of (BDI)SnOR and 2.68×10^{-6} mol of ferrocene was added to a sealable NMR tube with a 50 cm^3 headspace. The solution was submerged in a dry ice/ethanol bath, the gas inside the NMR tube was evacuated and CO_2 was introduced at a pressure of 1 atm. The reaction mixture was kept at 313.1 K in a thermostatted bath for 72 h and the **2**/**5** ratio was monitored by comparing the γ-C*H* ^{1}H NMR signal to the internal standard ferrocene. In order to ensure accurate integration, a 10s delay between 30° pulses was utilized (number of scans = 4, acquisition time = 4).

Computational Details. All the calculations were carried out using density functional theory (DFT) in the Gaussian 03 program.[30] Geometry optimization for the full complexes ((BDI)SnOR) was performed at the b3lyp level by using a double-ζ basis set (Lanl2dz) plus a d type polarization function (d exponent 0.183) along with the effective core potential (Lanl2 ECP)[48] for Sn atoms and 3-21 g for all other atoms. Geometry optimization for the model complexes (L$^\#$SnOR) was performed at the b3lyp level by using a double-ζ basis set (Lanl2dz) plus a d type polarization function (d exponent 0.183) along with the effective core potential (Lanl2 ECP)[48] for Sn atoms and 6-31+g* for all other atom. Single point calculations were carried on all the found saddle points with the larger basis set [4333111/433111/43] plus two d polarization function (d exponents 0.253 and 0.078) for Sn[49,50] and 6-31 g(d, p) for all the other atoms. Zero-point vibrational energy corrections were also included. All the transition structures (TS) were located on the potential energy surfaces and verified by one imaginary frequency. Intrinsic reaction coordinates (IRC) calculations confirmed the connectivity of TS with reactants and products.

Acknowledgment. The authors are grateful for the financial support from the EPSRC (LF, grant no EP/E032575/1).

Supporting Information Available: Cartesian coordinates and total energies of all the structures, basis set information for the large basis set single-point calculations, crystallographic data for **2b**, **2c**, **4**, and **6** (CIF), and full citation for ref 30. This material is available free of charge via the Internet at http://pubs.acs.org.

(48) Wadt, W. R.; Hay, P. J. *J. Chem. Phys.* **1985**, *82*, 284.

(49) Takagi, N.; Nagase, S. *Organometallics* **2007**, *26*, 469.

(50) *Gaussian Basis Sets for Molecular Calculations*; Elsevier: Amsterdam, 1984.